

Supporting Information

Miller et al. 10.1073/pnas.0913114107

SI Text

Experiment-Based $A\beta_{1-42}$ Model Construction: Linking Zn^{2+} Complexed N-Terminal and a β -Sheet Forming C-Terminal. We used three high-resolution solution NMR structures that are available for the N-terminal segment complexed with Zn^{2+} : The first is Zn^{2+} - $A\beta_{1-16}$, based on the Zirah model (S1) where Zn^{2+} binds to H6, E11, H13, and H14 [Protein Data Bank (PDB: 1ZE9)]; the second Zn^{2+} -human $A\beta_{1-28}$, based on the Gaggelli model (S2) where Zn^{2+} binds to D1, H6, E11, H13, and H14; and the third Zn^{2+} -rat $A\beta_{1-28}$, based on the Gaggelli model (S2) where Zn^{2+} binds to D1, H6, E11, and H14 in human $A\beta_{1-28}$. In addition, we constructed a model suggested by Minicozzi et al. (S3) based on X-ray absorption spectroscopy, in which Zn^{2+} interacts with four histidines (H13 and H14 of each two peptides). However, we extended the latter model by including Zn^{2+} binding to E11 of two peptides. The number of possible combinations for Zn^{2+} - $A\beta$ complex is large, and the stability and the population distribution of the possible conformers could change depending on concentration, temperature, and pH. Here we selectively constructed 12 polymorphic Zn^{2+} - $A\beta$ models, considering both parallel and antiparallel arrangements. Table 1 summarizes the 12 constructed models based on the experimental data.

Models M1–M5 were constructed directly from a combination of the Zirah model (S1) (PDB: 1ZE9) and Lührs model (S4) (PDB: 2BEG): M1 and M2 were arranged in a parallel organization, whereas M3–M5 in antiparallel organization. In M1, eight Zn^{2+} bind to eight $A\beta_{1-42}$ monomers, and in M2, only four Zn^{2+} bind to four monomers in the octamer (Fig. 1). This is the only $A\beta$ octamer model containing four Zn^{2+} . All others are “saturated,” binding to eight Zn^{2+} . M3 (Fig. 1), M4, and M5 (Fig. S1) differ in the β -sheet registration: M3 is shifted by two residues compared to M4, whereas M4 is shifted by two residues compared to M5. M3 has a maximum overlap of the hydrophobic region and therefore has strong β -sheet interactions as compared to M4 and M5.

Considering further possible zinc coordination patterns, we constructed six additional Zn^{2+} - $A\beta$ octamers M6–M11 (Fig. 1 and Fig. S2), based on the Gaggelli model (S2). M6–M9 arranged in a parallel organization, whereas M10 and M11 in antiparallel organization. Model M6 was derived from the homology model of the Zn^{2+} -rat $A\beta_{1-28}$ complex, using only the Zn^{2+} - $A\beta_{1-16}$ where each Zn^{2+} coordinates with D1, H6, E11, and H14. In the three models M7, M8, and M9, the Zn^{2+} coordinates with D1, H6, E11, H13, and H14 (S2), i.e., penta-coordinated with Zn^{2+} : M7 is a “hybrid” model, which was initially constructed from the simulated structure of M6. The additional Zn^{2+} -H13 coordination (as observed experimentally in Zn^{2+} -human $A\beta_{1-28}$ complex) was constrained and minimized prior to the simulations. M8 was constructed directly from the experiment (S2). M9 is a hybrid model, which was derived from the simulated structure M1. The additional Zn^{2+} -D1 coordination was initially constrained and minimized before the simulations. Finally, M10 and M11 were constructed to test the penta-coordinated Zn^{2+} - $A\beta$ complexes in antiparallel β -sheet arrangements. M10 and M11 differ in the β -sheets twisting angles in the initial conformation.

Finally, to consider not only intrapeptide zinc binding, but also interpeptide zinc binding, model M12 was constructed, based on the Minicozzi model (S3), in antiparallel arrangement where $4Zn^{2+}$ bind H13 and H14 and $4Zn^{2+}$ bind E11 of each two peptides (Fig. 1). It should be noted that M12 was constructed using the Lührs model (S4) for the 17–42 segment. However, Tycko’s model (S5) may also be used to construct M12. The main

difference between the Tycko and Lührs models is the U-turn shape. Future work will investigate whether the different in the U-turn shape can lead to polymorphism as recently demonstrated for $A\beta_{17-42}$ (S6).

Geometrical Match and Interactions in the Zn^{2+} - $A\beta_{1-16}$ Region. The three different coordination intrapeptide zinc-binding NMR structures affect the overall shapes of the Zn^{2+} - $A\beta$ complex in the 1–16 regions. At the Zn^{2+} - $A\beta_{1-42}$ monomer level, variations in both N-terminal and C-terminal regions provide large ensembles. However, in the Zn^{2+} - $A\beta_{1-42}$ oligomeric state, the Zn^{2+} - $A\beta_{1-16}$ shapes are constrained by the β -strands arrangement. In mature fibrils, the distance between two adjacent β -strands in two β -sheets is ~ 5 Å (and ~ 10 Å for two alternative β -strands). Thus, the only possibility to construct the Zn^{2+} - $A\beta_{1-16}$ regions with the β -strands is with one plane of the β -strands, separated by at least one uncoordinated β -strand.

While testing possible arrangements of the Zn^{2+} - $A\beta_{1-16}$ with the β -strands for the Zirah and Gaggelli models (S1, S2), we found that the Zirah model (PDB: 1ZE9) (S1) has complementary shapes with tightly packed geometry between two nearby Zn^{2+} - $A\beta_{1-16}$ peptides. The optimal orientation between two nearby Zn^{2+} - $A\beta_{1-16}$ peptides (Fig. 2A) was obtained using the docking program PatchDock (S7). PatchDock, a geometry-based molecular docking algorithm was used to probe possible ways of association of the Zn - $A\beta_{1-16}$ complex of the NMR structure (PDB: 1ZE9). Hydrogen atoms were not used in the docking. In order to decrease the geometrical clashes, the maximal allowed penetration between the molecular surfaces was set to -1.5 Å.

Surprisingly, from thousands of possible poses, only only were generated, with five obtaining additional intermolecular interaction of Asp7 with Zn^{2+} of neighboring Zn^{2+} - $A\beta_{1-16}$ complexes (Fig. S4). The two highest ranking docking poses are similar with the backbone carbonyl of Asp7 directly pointing to Zn^{2+} , with a distance of 3.81 Å.

The geometrical match of two Zn^{2+} - $A\beta$ complexes does not exist for the Gaggelli model (S2) where Zn^{2+} binds five intramolecular ligands (M8 and M9). However, in the Gaggelli model M6, where Zn^{2+} binds four intramolecular ligands, intermolecular Asp7-COO⁻- Zn^{2+} interactions also exist. M7 is a hybrid of M6, and thus three of the six Asp7-COO⁻- Zn^{2+} distances show strong intermolecular interactions.

Molecular Dynamics (MD) Simulations Procedure. Constant temperature (300 K) and constant pressure (1 atm) were controlled by the Hoover method (S8), using the CHARMM package or by Langevin thermostat with a damping coefficient of 10 ps⁻¹, using the NAMD program. For simulations using the NAMD program (S9), the Langevin piston method (S9–S11) with a decay period of 100 fs, and a damping time of 50 fs was used to maintain a constant pressure of 1 atm. The short-range van der Waals (VDW) interactions were calculated using the switching function, with a twin range cutoff of 10.0 and 12.0 Å. Long-range electrostatic interactions were calculated using the particle mesh Ewald method with a cutoff of 12.0 Å for all simulations. The equations of motion were integrated using the leapfrog integrator with a step of 1 fs. All initial $8Zn^{2+}$ - $8A\beta_{1-42}$ oligomers and the $4Zn^{2+}$ - $8A\beta_{1-42}$ oligomer were minimized and then solvated in a TIP3P water box with a minimum distance of 10–15 Å from any edge of the box to any $A\beta$ atom. Any water molecule within 2.5 Å of the $A\beta$ was removed. Counterions (Na⁺) were added at random

locations to neutralize the charge of $8\text{Zn}^{2+}-8\text{A}\beta_{1-42}$ and $4\text{Zn}^{2+}-8\text{A}\beta_{1-42}$.

The solvated systems were minimized for 2,000 conjugated gradient steps, with the distance between the β -sheets fixed in the range 2.2–2.5 Å. The VDW parameters of Zn^{2+} ion are taken from CHARMM27 force field, and all Zn^{2+} -ligands distances were constrained to their NMR evaluated distances, both along the minimization process and during all dynamics simulation timescales. Counterions, peptides, and water molecules were all allowed to move. The hydrogen atoms were constrained to the equilibrium bond using the SHAKE algorithm (S12). The minimized solvated systems were minimized for additional 5,000 conjugate gradient steps at 250 K, where all atoms were allowed to move. Then, the systems were heated from 250 to 300 K for 300 ps and equilibrated at 300 K for 300 ps. Simulations ran for 20 ns and structures were saved every 10 ps for analysis.

Generalized Born Method with Molecular Volume (GBMV). In the GBMV calculations, the dielectric constant of water was set to 80.0 and no distance cutoff was used. The hydrophobic solvent-accessible surface area term factor was set to $0.00592 \text{ kcal/mol} \cdot \text{Å}^2$. Each conformer is minimized for 1,000 cycles and the conformation energy is evaluated by grid-based GBMV. The minimization does not change the conformations of each conformer, but only relaxed the local geometries due to thermal fluctuation which occurred during the MD simulations.

A total of 11,000 conformations (1,000 conformations for each of the 11 examined conformers) were used to construct the free-energy landscape of the $8\text{Zn}^{2+}-8\text{A}\beta_{1-42}$ oligomer and to evaluate the conformer probabilities by using Monte Carlo (MC) simulations. In the first step, one conformation of conformer i and one conformation of conformer j are randomly selected. Then, the Boltzmann factor is computed as $e^{-(E_j-E_i)/KT}$, where E_i and E_j are the conformational energies evaluated using the GBMV calculations for the conformation i and j , respectively, K is the Boltzmann constant, and T is the absolute temperature (298 K used here). If the Boltzmann factor value is larger than the random number, the move from conformation i to conformation j is allowed. After 1 million steps, the conformations visited for each conformer were counted. Finally, the relative probability of

conformer n was evaluated as: $P_n = N_n/N_{\text{total}}$, where P_n is the population of conformer n , N_n is the total number of conformations visited for the conformer n , and N_{total} is the total steps. The advantages of using the MC simulations to estimate conformer probability rely on the facts that the MC simulations have good numerical stability and allow transition probabilities among several conformers to be controlled.

Using all 11 conformers (not including M2) and 11,000 conformations (1,000 for each conformer) generated from the MD simulations, we estimate the overall stability and populations for each conformer based on MC simulations with the energy landscape computed with GBMV for all conformers. For the complex kinetics of amyloid formation, this group is likely to represent only a very small percentage of the ensemble. Nevertheless, the carefully selected models cover the most likely organizations.

Conformational Stability of Constructed $4\text{Zn}^{2+}-8\text{A}\beta_{1-42}$ and $8\text{Zn}^{2+}-8\text{A}\beta_{1-42}$ Oligomers. The relative conformational stabilities of the oligomers were measured by rmsd of the C-terminal region (residues Leu17–), the N-terminal region (residues Ala2–Gln15), and for the U-turn region (residues Glu22–Gly29) with respect to the initial minimized structure throughout the simulations. We also followed the change in the Asp7– Zn^{2+} distance, i.e., the averaged distance of the two C = O bonds of Asp7 to the Zn^{2+} in the adjacent peptide.

Our simulations indicated that the tested oligomers are structurally stable, suggesting that they could exist under appropriate conditions. Among the 12 constructed models, six were arranged in a parallel organization (M1, M2, M6, M7, M8, and M9). Fig. S6 demonstrates the rmsds of these models. M1 and M2 have relatively smaller rmsds for the C-terminal regions, indicating that the large contact surface in the N termini also affects the overall oligomer structural stability. Overall, for all parallel models both the N termini and the U-turn rmsds indicate the stability of these regions. Six constructed models were arranged in an antiparallel organization (M3, M4, M5, M10, M11, and M12). Among these, we compared only the four most stable models M3, M4, M11, and M12. Both the C termini and the U-turn rmsds are small, indicating their structural stability (Figs. S7 and S8).

- Zirah S, et al. (2006) Structural changes of region 1-16 of the Alzheimer disease amyloid betapeptide upon zinc binding and in vitro aging. *J Biol Chem* 281:2151–2161.
- Gaggelli E, et al. (2008) NMR studies of the Zn^{2+} interactions with rat and human beta-amyloid (1-28) peptides in water-micelle environment. *J Phys Chem B* 112:100–109.
- Minicozzi V, et al. (2008) Identifying the minimal copper- and zinc-binding site sequence in amyloid-beta peptides. *J Biol Chem* 283:10784–10792.
- Luhns T, et al. (2005) 3D structure of Alzheimer's amyloid-beta(1-42) fibrils. *Proc Natl Acad Sci USA* 102:17342–17347.
- Petkova AT, Yau WM, Tycko R (2006) Experimental constraints on quaternary structure in Alzheimer's beta-amyloid fibrils. *Biochemistry* 45:498–512.
- Miller Y, Ma BY, Nussinov R (2009) Polymorphism of Alzheimer's a-beta(17-42) p3 oligomers: The importance of the turn location and its conformation. *Biophysical J* 97:1168–1177.
- Schneidman-Duhovny D, Inbar Y, Nussinov R, Wolfson HJ (2005) PatchDock and SymmDock: Servers for rigid and symmetric docking. *Nucleic Acids Res* 33:W363–W367.
- Hoover WG (1985) Canonical dynamics: Equilibrium phase-space distributions. *Phys Rev A* 31:1695–1697.
- Kale L, et al. (1999) NAMD2: Greater scalability for parallel molecular dynamics. *J Comput Phys* 151:283–312.
- Martyna GJ, Tobias DJ, Klein ML (1994) Constant pressure molecular dynamics algorithms. *J Chem Phys* 101:4177–4189.
- Feller SE, Zhang YH, Pastor RW, Brooks BR (1995) Molecular dynamics simulations at constant pressure: The Langevin Piston method. *Journal of Chemical Physics* 103:4613–4621.
- Ryckaert JP, Ciccotti G, Berendsen HJC (1977) Numerical-integration of Cartesian equations of motion of a system with constraints—Molecular-dynamics of N-alkanes. *J Comput Phys* 23:327–341.

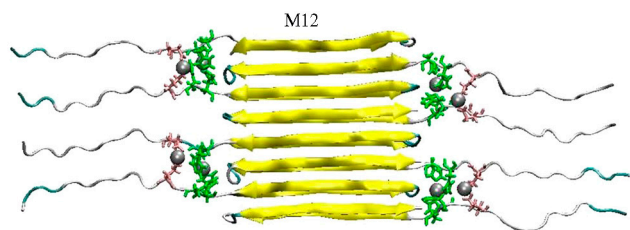


Fig. S3. Figure illustrates that the experimental, solution NMR-based conformers of the Zn^{2+} complexed with residues 1–16 (the N-terminal region) fit well with the experiment-based structure for the remainder of the $A\beta$ (residues 17–42), and consequently can be linked to create models of the full-length $A\beta_{1-42}$ complexed with Zn^{2+} . The Zn^{2+} -coordinated N-terminal coordinates are taken from Miniccozzi (S3). The coordinates of residues 17–42 are taken from the Lührs oligomers (S4). M12 is arranged in antiparallel organization in which four Zn^{2+} interact with H13 and H14 of each two peptides and four Zn^{2+} interact with E11 of each of the same two peptides.

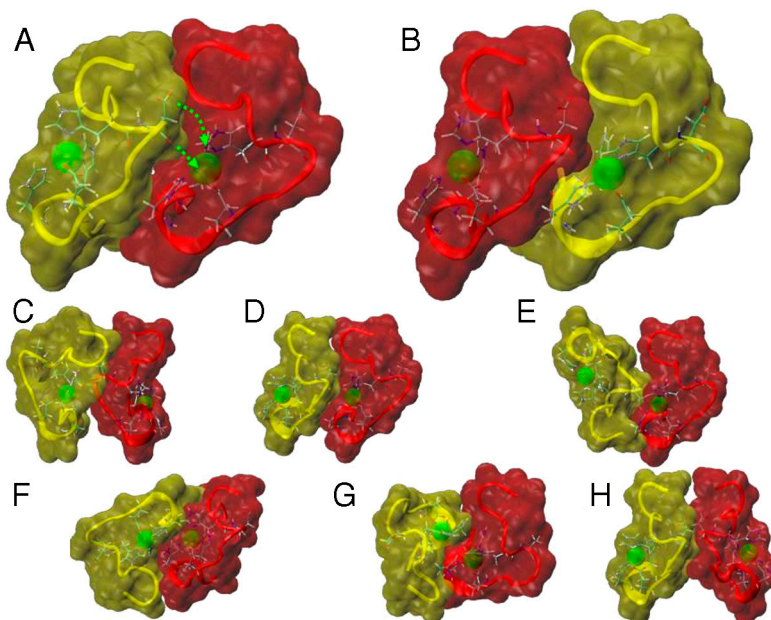


Fig. S4. Eight possible poses generated from the PatchDock program (S7). Five poses (A–E) exhibit additional intermolecular interaction of Asp 7 with Zn in nearby Zn^{2+} - $A\beta_{1-16}$ complexes using dimers of Zirah model (S1) (PDB: 1ZE9).

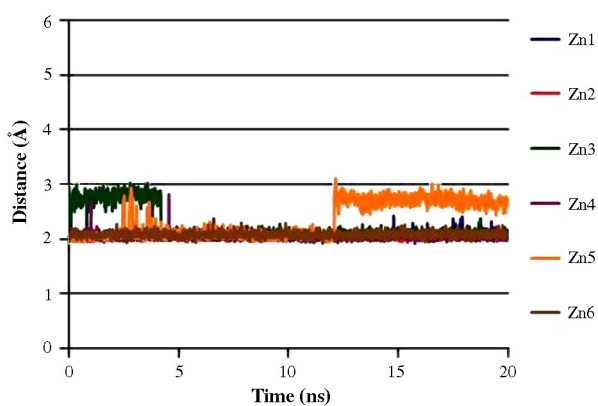


Fig. S5. Six Asp7-COO⁻- Zn^{2+} distances for the antiparallel M3 model demonstrate strong interactions during all time of the simulations.

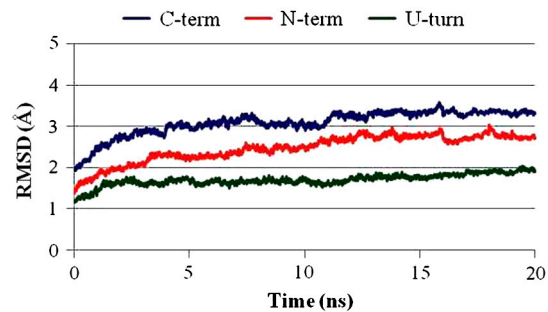


Fig. S8. Figure shows that the antiparallel model M11 proposed in this work for Zn^{2+} binding to $A\beta_{1-42}$ is stable as indicated by its rmsds. The rmsds are computed separately for the three parts of the oligomer: C-terminal (residues 17–40), N-terminal (residues 2–15), and U-turn (residues 22–29).

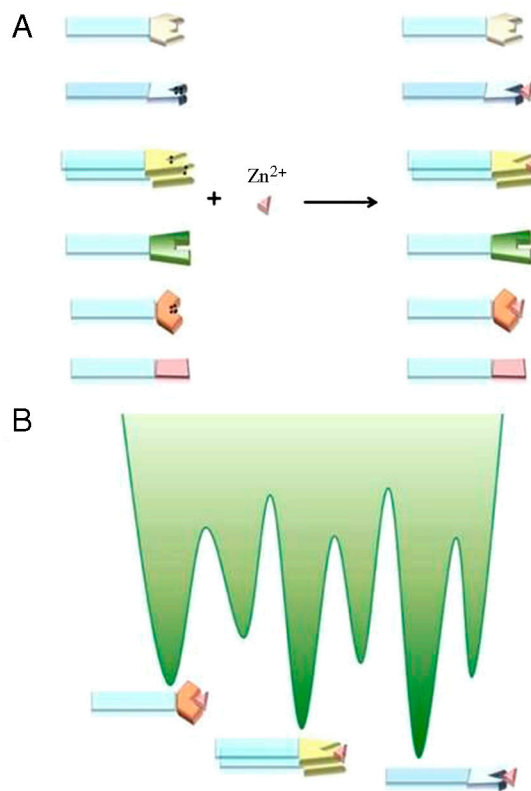


Fig. S9. Schematic illustration of the Zn^{2+} binding to different N-terminal conformations in $A\beta$ amyloids via conformational selection. The monomers interacting with Zn^{2+} are not consecutive in the oligomer organization. In between, noncoordinating monomers may be arranged in parallel or in antiparallel organization. Figs. S1–S3 provide detailed organizations.